Fusion Engineering and Design 89 (2014) 847–852

Contents lists available at ScienceDirect

Fusion Engineering and Design

journal homepage: www.elsevier.com/locate/fusengdes

RF calculation and thermal-stress analysis of the ECRH launcher on EAST tokamak

Yunying Tang[a,b,*], Xiaojie Wang[a], Fukun Liu[a], Bo Li[a], Handong Xu[a], Weiye Xu[a], Wei Wei[a], Dajun Wu[a]

[a] Institute of Plasma Physics, Chinese Academy of Sciences, Shushanhu Road 350, Hefei 230031, Anhui, China
[b] University of Science and Technology of China, Jinzhai Road 96, Hefei 230026, Anhui, China

HIGHLIGHTS

- The new constructing 140 GHz/1 MW/1000 s ECRH system was briefly introduced and the structure of ECRH launcher was detailedly described.
- The transmission characteristics of the RF propagation inside the launcher were calculated and the Gaussian beam radius in the resonance layer of plasma was optimized.
- Temperature distribution and thermal-stress of mobile mirror were analyzed.
- The inner equivalent diameter of water channel in the mobile mirror and the suggested water velocity were analyzed.

ARTICLE INFO

Article history:
Received 19 December 2013
Received in revised form 25 March 2014
Accepted 29 April 2014
Available online 21 May 2014

Keywords:
ECRH launcher
Gaussian beam
Thermal stress
EAST

ABSTRACT

EAST is a medium sized superconducting tokamak with major radius $R = 1.8$ m, minor radius $a = 0.45$ m, plasma current $I_p \leq 1$ MA, toroidal field $B_T \leq 3.5$ T and expected plasma pulse length up to 1000 s. An electron cyclotron resonance heating (ECRH) launcher for four-beam injection is being installed on EAST tokamak. Four electron cyclotron wave beams which are generated from four sets of 140 GHz/1 MW/1000 s gyrotrons will be injected into the plasma by the spherical focusing mirrors and plane mobile mirrors. The focusing mirrors are spherical to focus Gaussian beams after reflection. Four plane mobile mirrors independently steer continuously in the poloidal and toroidal direction controlled by motors. With the suitable distance between mirrors and appropriate focal length of focusing mirror, the beam radius in the resonance layer of plasma is 31.145 mm. The heat from plasma radiation and metal losses is loaded on the mobile mirror. In order to decrease the temperature and thermal stress, the inner equivalent diameter of water channels is 8 mm and the suggested water velocity is 4 m/s.

1. Introduction

As one of the main auxiliary heating methods in controllable nuclear fusion experiment, ECRH is effective and attractive on the plasma heating. The advantage of ECRH is obvious, such as high coupling efficiency and fine localized power deposition. At present, ECRH system has been installed or applied to a variety of tokamaks, for instance, Tore Supra [1], ASDEX-U [2], JT-60U [3], FTU [4], and DIII-D [5]. An ECRH system is being designed to deliver 4 MW continuous wave (CW) at Institute of Plasma Physics, Hefei. The physics applications of EAST ECRH system are localized electron heating, electron cyclotron current drive (ECCD), local MHD [6] control, plasma start-up assist and developing high parameter steady state discharge operation mode.

The planned system is composed of an equatorial launcher using four 1 MW/1000 s gyrotrons working at 140 GHz (Fig. 1). Four transmission lines are inserted simultaneously into the EAST tokamak via one 518 mm × 960 mm window port on account of the number and sizes restriction of window ports. Each transmission line is constituted by a series of microwave device, such as miter bends, polarizers [7], CVD window [8], and gate valve. Two polarizers in each transmission line control the polarization of injected beam, with the result that pure X-mode power injection can be achieved for all injection angles.

When EC wave beam is emitted from the open end of a corrugated waveguide of the transmission line to vacuum environment

* Corresponding author at: Institute of Plasma Physics, Chinese Academy of Sciences, Shushanhu Road 350, Hefei 230031, Anhui, China. Tel.: +86 551 65593291; fax: +86 551 65593332.
E-mail address: yytang@ipp.ac.cn (Y. Tang).

http://dx.doi.org/10.1016/j.fusengdes.2014.04.070
0920-3796/

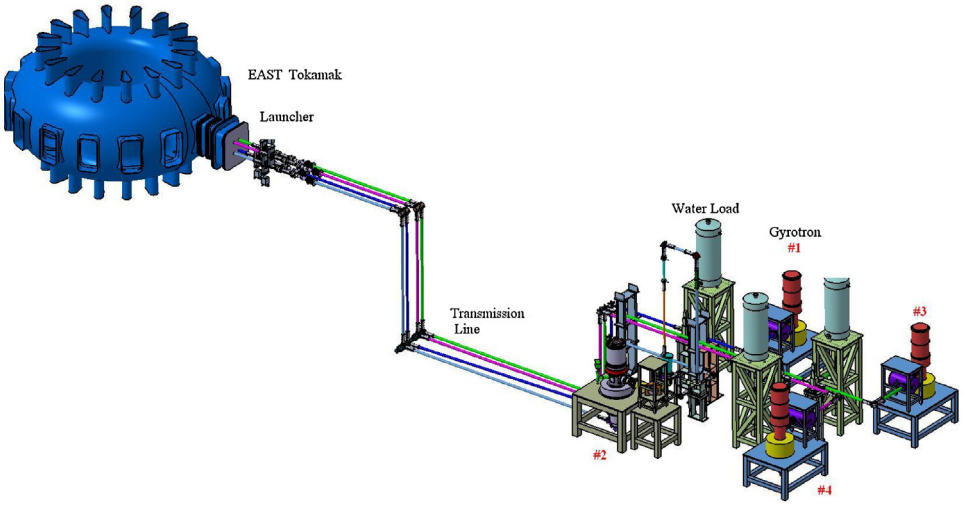

Fig. 1. The schematic layout of EAST ECRH system.

in the launcher, the HE_{11} mode wave changes to Gaussian beam. In order to get reasonable beam radius in the plasma, the properties of the Gaussian beam and the calculation of the RF propagation should be analyzed.

Owing to the operation in long pulse and resistive losses of the mirror material, the mirrors absorb part of power and therefore the temperature of them will rise rapidly. Once the mechanical stress resulted from temperature exceeds bearing scope of materials, the mirrors will be destroyed. In order to estimate the thermal performance of the mirrors, the peak temperature on the mirrors must be estimated. The allowable temperature increase is limited by the stress accompanied with the thermal expansion of the mirrors.

2. Structure of the launcher

The launcher of EAST ECRH system mainly consisting in optical mirrors, mirror steering mechanisms, cooling and support structures is installed on the window port of the tokamak by a plug-in assembly (Fig. 2).

Optical mirrors are four focusing mirrors and four mobile mirrors. The size of the mirrors is chosen to ensure that tiny Gaussian beam power falls outside their edges. The dimensions of the focusing mirror are 127 mm × 90 mm and mobile mirror sizes are 170 mm × 113 mm. The beam width is about 15 mm and therefore there is at least 99.99% Gaussian beam power intercepted by reflecting surfaces of mirrors. Each mirror is made of two materials which are copper and stainless steel. The material of the mirror surface is copper with high thermal conductivity. The copper is inlaid in the stainless steel which increases the mechanical strength of the mirror.

4 MW power generated from four sets of 140 GHz/1 MW/1000 s gyrotrons is injected into the plasma as Gaussian beams. Four Gaussian beams are injected into four fixed spherical focusing mirrors independently, and then injected into appointed region in the plasma by four plane mobile mirrors. When Gaussian beams eject from corrugated waveguides, because of Gaussian beams properties their intensities are diverging along the transmission route. Meanwhile, the focusing mirrors are at angles of 45° with respect to the incident beams, therefore they should be ellipsoidal to achieve non-astigmatic beams after reflection. The astigmatism due to the use of spherical mirrors has been estimated to be unimportant and hence the spherical focusing mirrors have been chosen to facilitate the manufacturing process. The plane mobile mirrors just change the transmitting direction of beams, while the properties of Gaussian beam remain unchanged. Each mobile mirror controlled by horizontal motor and vertical motor steers independently in the poloidal and toroidal direction, respectively. The rotation ranges of poloidal angle and toroidal angle are shown in Fig. 3 for a limiter configuration. The major radius of EAST is 1800 mm and minor radius is 450 mm. The mirror is 3000 mm distant from the center of EAST. Each mirror offsets 300 mm in the poloidal direction and 100 mm in the toroidal direction. Supposing upward angle is positive, the range of poloidal angle is from −25° to 5° and the range of toroidal angle is from −30° to +30°.

The power capacity of the launcher is 4 MW when four transmission lines are all in long pulse full-power operation. Meanwhile, the mobile mirrors are working in drastic and severe conditions caused by their locations in the direct view of the plasma. In order to minimize power deposition and guarantee the required lifetime of mirrors, the cooling structure to the mirrors is very important and necessary. The appropriate cooling structure maintains the temperature of mirrors within the operational range.

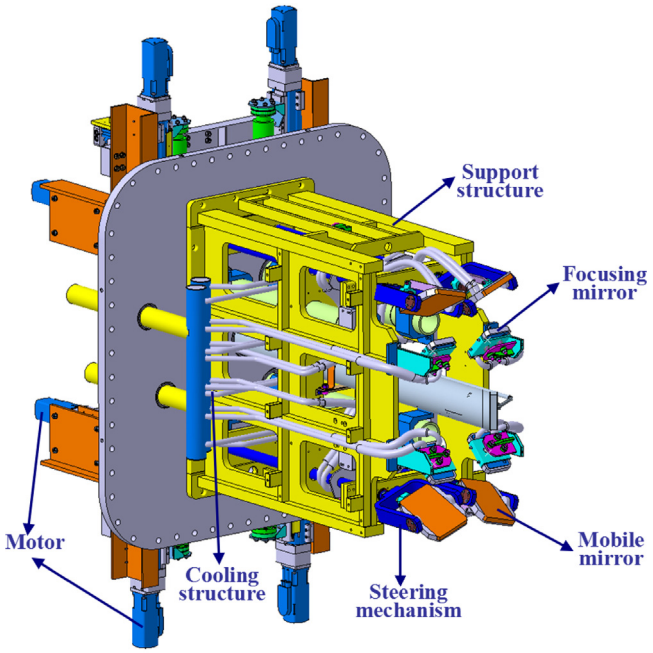

Fig. 2. The overall layout of ECRH system launcher.

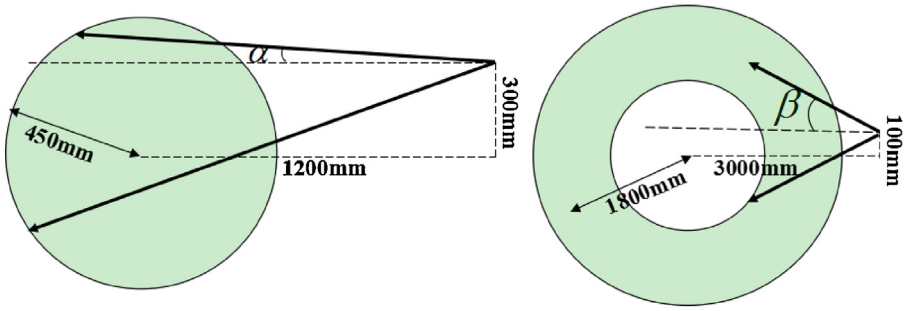

Fig. 3. The rotation ranges of poloidal angle (left) and toroidal angle (right).

3. Properties analysis

3.1. The calculation of the RF propagation inside the launcher

The Gaussian beams emitted by corrugated waveguides are focused by the spherical focusing mirrors before being directed into the plasma by the mobile mirrors (Fig. 4). The beam waist r_0 situated at the waveguide port is the minimum radius, given by [9]

$$r_0 \cong 0.42 \times a \tag{1}$$

where a (=31.75 mm) is the inner radius of the corrugated waveguide.

Defining Z as the distance along the beam, beam radius $r(Z)$ perpendicular to the beam can be calculated according to [10]:

$$r(Z) = r_0\sqrt{1 + \left(\frac{cZ}{2\pi f r_0^2}\right)^2} \tag{2}$$

where c is the speed of light and f is the frequency.

Ignoring the astigmatism and hence assuming perfect Gaussian beams following reflection in the focusing mirrors, the parameters of these beams are described by the following equations [11]:

$$Z_{\mathrm{wr}} = F + \frac{(Z_1 - F)F^2}{(Z_1 - F)^2 + (2\pi r_0^2/\lambda)^2} \tag{3}$$

$$r(Z_{\mathrm{wr}}) = \frac{Fr_0}{\sqrt{(F - Z_1)^2 + (2\pi r_0^2/\lambda)^2}} \tag{4}$$

where F is the focal length of the spherical focusing mirrors which influences the properties of Gaussian beams, Z_{wr} is the distance from focusing mirror to the waist behind focusing mirror, $r(Z_{\mathrm{wr}})$ is the beam waist radius at this point, $\lambda = c/f$ is the wavelength. With the beam waist radius $r(Z_{\mathrm{wr}})$, the beam radius $r(Z_p)$ in the resonance layer of plasma can be got in Eq. (2).

The distance Z_1 from corrugated waveguide to focusing mirror and focal length F of spherical focusing mirror are unknown quantities. In order to get appropriate $r(Z_p)$ which should be relatively stable when there are small changes of focal length F and transmitting distance Z_1, a series of optimizations are made (Fig. 5).

In the optimizations, the value of Z_1 ranges from 200 mm to 350 mm and the range of F is from 100 mm to 800 mm. In order to get the effect of focal length F, the case of plane mirror (i.e. no focusing) is also presented for comparison. From the optimized results, with an invariable Z_1, the values of beam radius $r(Z_p)$ in the resonance layer of plasma change large when focal length (F) changes from 100 mm to 500 mm, while $r(Z_p)$ are almost the same when focal length (F) changes from 500 mm to 800 mm. With the increasing of Z_1, the beam radius $r(Z_p)$ does not change obviously with the same focal length (F). The beam radius $r(Z_p)$ in the resonance layer of plasma mainly depends on focal length (F). Considering the optimized results and the restriction on the size of EAST window port, all the parameters of optical transferring in the launcher are decided in Table 1.

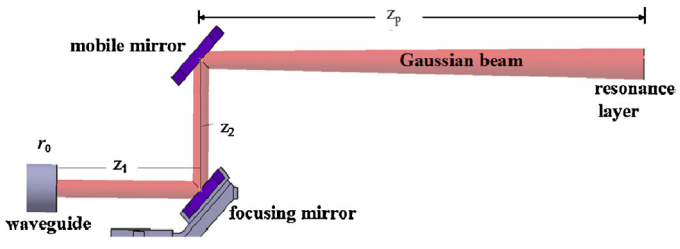

Fig. 4. The transferring route of Gaussian beam in the launcher. Z_1 is the distance from corrugated waveguide port to focusing mirror, Z_2 is the distance from focusing mirror to mobile mirror, and Z_p is the shortest distance from mobile mirror to the resonance layer of plasma. Due to the dimension restriction of EAST window port, Z_2 (=140 mm) and Z_p (=1200 mm) are decided.

3.2. Thermal-stress analysis of mobile mirrors

The metal focusing mirrors and mobile mirrors will absorb part of power when Gaussian beams are injected into them. The ideal absorption coefficient on metallic surface of launcher, with electric field parallel and perpendicular to the plane of incidence (respectively α_{E} and α_{H}) are described by the following equations [12]:

$$\alpha_{\mathrm{E}} = \frac{4}{\cos\theta} \cdot \frac{R_s}{Z_0} \tag{5}$$

$$\alpha_{\mathrm{H}} = 4\cos\theta \cdot \frac{R_s}{Z_0} \tag{6}$$

where

$$R_s = \sqrt{\frac{\pi f \mu_0}{\sigma}} \tag{7}$$

is the surface resistance of the metal, θ is the incidence angle of Gaussian beam, $Z_0 = \mu_0/\varepsilon_0$ is the impedance of vacuum, μ_0 is the permeability of the vacuum and σ is conductivity of the metal. The maximal absorption coefficient of incident power is 0.353%, assuming that $\theta = 45^\circ$ and $\sigma = 10^7\ \Omega^{-1}\ \mathrm{m}^{-1}$ with the conservative value for copper.

Table 1
Quasi-optical parameters for launcher design.

Term	a	r_0	Z_1	Z_2	Z_{wr}	F
Value (mm)	31.75	13.335	240	140	234	700
Term	Z_p	$r(Z_1)$	$r(Z_2)$	$r(Z_{\mathrm{wr}})$	$r(Z_p)$	
Value (mm)	1200	14.68	13.635	13.425	31.145	

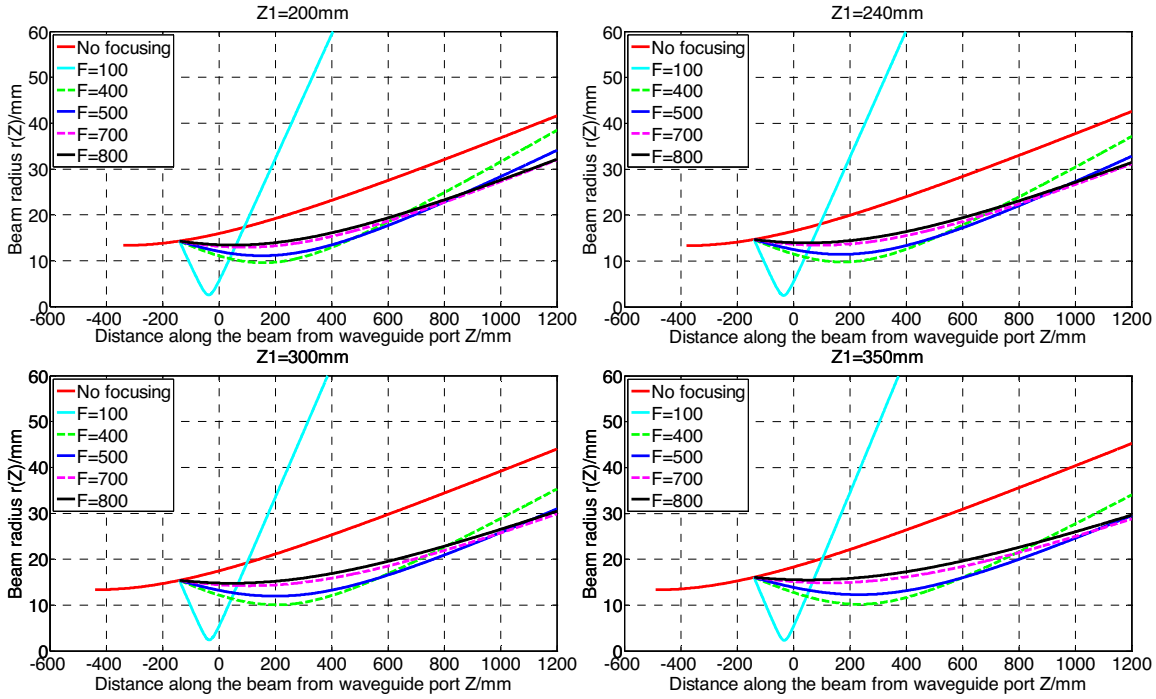

Fig. 5. The beam radius as a function of propagation distance for different possible choices of shaping mirror focal length and distance from waveguide termination to focusing mirror (increasing from plot1 to plot4). The positions of the focusing and steering mirrors as well as the plasma center are located in $Z = -140$ mm, 0 mm and 1200 mm, respectively.

The absorption power P_{loss} = 3.53 kW is Gaussian distribution on each mirror [13]:

$$I(r,z) = \frac{P_{loss}}{\pi r^2(Z)} \exp\left(-\frac{r^2}{r^2(Z)}\right) \tag{8}$$

where r is the distance perpendicular to the beam, and $r(Z)$ is the beam radius on the mirrors. In the center position of mirror, the peak load value is about 6 MW/m^2.

The focusing mirrors are kept away from the radiation of plasma by shutter but not mobile mirrors, therefore, the power deposited on the mobile mirrors is more than on focusing mirrors. The deposited power density of plasma is about 1.08 MW/m^2 on mobile mirrors, when all possible radiation power (44.3 MW) of future EAST tokamak is considered. Therefore, the cooling requirement to mobile mirrors is higher. If mobile mirrors meet cooling requirement, focusing mirrors which have similar cooling structure will be certainly satisfied. The thermal analysis of mobile mirrors is described as follows.

Under long pulse operation, the mobile mirror temperature will increases rapidly on account of metal losses if no active cooling is implemented, especially in the center position of mirror where the peak load value is about 7.08 MW/m^2. Consequently, the mirrors are designed to be cooled actively. The mirror structure made of copper and stainless steel is shown in Fig. 6. The inlet and outlet of cooling water are shown in the middle of Fig. 6. The cooling channels (shown on the right of Fig. 6) are situated in the copper body so that the contact area between copper and water is extensive. The water can take the deposited power away quickly based on the advantage of the high thermal conductivity of the copper. The thickness of copper and stainless steel is the critical design parameters. The thicker the copper is, the better cooling effect is; however, the thickness of stainless steel decides the strength of mirror. After some estimations and simulations by using the finite element code ANSYS, the thicknesses of copper and stainless steel are 15 mm and 5 mm, respectively.

The heat transfer coefficient defines the ease with which heat passes from one material to another, usually from a solid to a fluid. It means that, in the mirror model of Fig. 6, the heat transfer coefficient defines the ease of heat passing from copper surface to cooling water. The unit of heat transfer coefficient is W/m^2 K, where the area is the copper surface that is in contact with the cooling water and the temperature is the difference between the copper temperature and the water inlet temperature. The heat transfer coefficient is defined h and gotten by Dittus–Boelter equation [14]:

$$Nu = 0.023 Re^{0.8} Pr^{0.4} \tag{9}$$

where the Nusselt number Nu and the Reynolds number Re are defined by

$$Nu = \frac{hd}{k} \tag{10}$$

$$Re = \frac{\upsilon_f d}{\nu} \tag{11}$$

υ_f is the average water velocity, d is equivalent diameter of cooling channel, k is thermal conductivity of the water, ν is the viscosity of water, Pr is the Prandtl number that is about 5.42 when the temperature is 30 °C.

Considering Eqs. (9)–(11) together, the relationship between heat transfer coefficient h and water velocity υ_f under the different equivalent diameters of the cooling channels which are 6, 7, 8 and 9 mm can be obtained. In Fig. 7, it shows that the heat transfer coefficients increase strongly with water velocity and they are not affected very much by the inner equivalent diameter of cooling channels. In the thermal analysis, the inner equivalent diameter is chosen 8 mm, and the water velocity is 2 m/s, hence the heat transfer coefficient is 10.6 kW/m^2 K.

The relationship between the thermal stress and the temperature is estimated by ANSYS software. A 3D analysis is performed. The metal losses and radiation flux are applied with a function distributed on the surface of copper and convection is loaded on the area of cooling channels. The temperature distribution and the

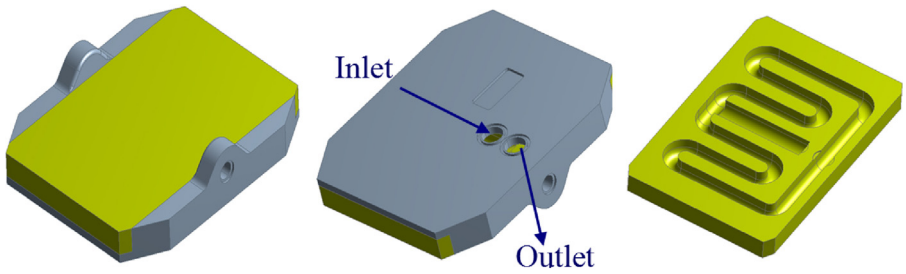

Fig. 6. The structure of launcher mirror (left), the backfaces of mirror structure (middle) and the cooling channels in the copper body of the mobile mirror (right).

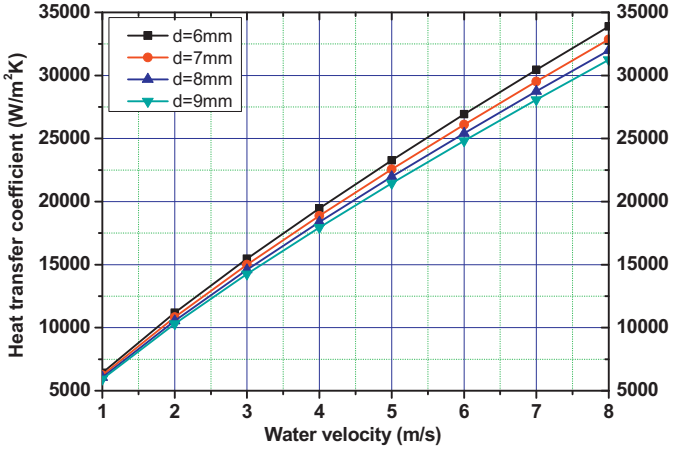

Fig. 7. The heat transfer coefficient in the different inner equivalent diameter of cooling channels.

thermal stress profile are shown in Figs. 8 and 9, respectively. Water is used in the cooling system of the launcher and a uniform initial temperature of 30 °C is assumed. The absorption power owing to metal loss of mobile mirror is Gaussian distribution and has been shown in Eq. (8). The temperature distribution on the surface of mirror keeps consistency with the equation. The peak temperature on the mobile mirror is 296.64 °C, which is located in the center of the mirror surface where the peak heat load is deposited. The peak thermal stress is 178.1 MPa at the corner of cooling channels adjoining the stainless steel side. The areas of peak stress are very small, just several points as shown. The thermal stress in the vast majority of areas is smaller than 100 MPa. The copper and stainless steel tensile strengths are 245 MPa and 480 MPa, respectively, consequently the stress on copper and stainless steel is acceptable.

Supposing that the total heat on the mobile mirror is absorbed by the cooling water, the water temperature increment can be gotten by equation:

$$Q = cmt \tag{12}$$

where Q is total heat on the mobile mirror, c is specific heat of water, m is the mass of water and t is temperature increment of water. The temperature increment of water is 45 °C in the thermal analysis, when the inner equivalent diameter is 8 mm and the water velocity is 2 m/s (Fig. 10). From Fig. 10, the temperature increments decrease quickly when the water velocity changes from 1 m/s to 4 m/s. However, they decrease slowly when the water velocity is greater than 4 m/s in all different inner equivalent diameters. Because of such a low temperature increment of 23 °C, the inner equivalent diameter of 8 mm is selected for the mobile mirror, when the suggested water velocity is 4 m/s. Based on the present design, the outlet water temperature is 53 °C for the mobile mirror, which is far below the boiling point of water in the normal pressure.

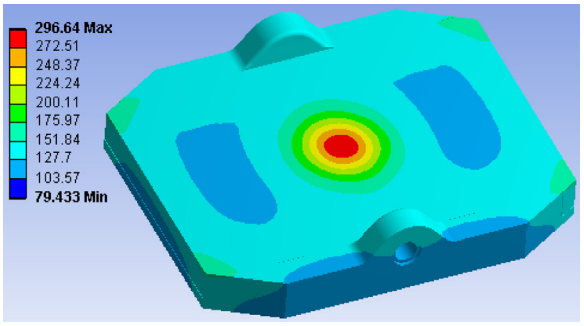

Fig. 8. The temperature distribution of the mobile mirror.

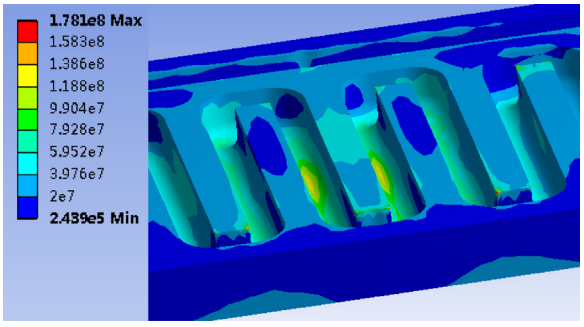

Fig. 9. The thermal stress (in Pa) of the mobile mirror.

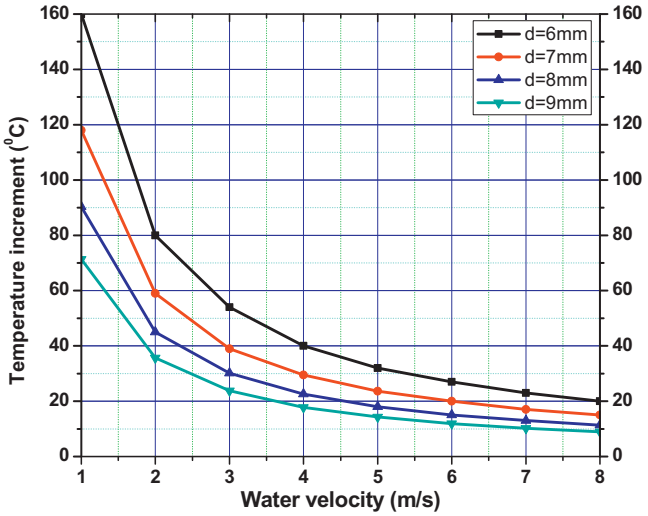

Fig. 10. Temperature increment of cooling water.

4. Conclusions

In the presented design, the launcher is mainly composed by four spherical focusing mirrors and four plane mobile mirrors. The beam radius in the resonance layer of plasma is 31.145 mm after RF beam is reflected sequentially by two mirrors, which is suitable for localized MHD control. According to the analysis of thermal behavior and structural integrity, the maximum temperature in the center of the mobile mirror is 296.64 °C and the subsequent thermal stresses do not deteriorate it. They are expected to withstand EAST thermal loads.

Further study should be carried out and the electromagnetic force of the mobile mirror needs to be taken into account. Combining the thermal stress and electromagnetic force, the analysis of the mirror is more close to the real situation in EAST tokamak.

The 140 GHz/1 MW/1000 s ECRH system on EAST tokamak is being fabricated and will be operated in the next EAST experiment. In view of new experiments and testing of new techniques, the ECRH system will certainly increase the capabilities of EAST tokamak.

References

[1] C. Darbos, R. Magne, A. Arnold, H.O. Prinz, M. Thumm, F. Bouquey, et al., The 118-GHz electron cyclotron heating system on Tore Supra, Fusion Sci. Technol. 56 (2009) 1205–1218.
[2] D. Wagner, J. Stober, F. Leuterer, F. Monaco, M. Münich, D. Schmid-Lorch, et al., Recent upgrades and extensions of the ASDEX upgrade ECRH system, J. Infrared Milli Terahz Waves 32 (2011) 274–282.
[3] T. Suzuki, S. Ide, K. Hamamatsu, A. Isayama, T. Fujita, C.C. Petty, et al., Heating and current drive by electron cyclotron waves in JT-60U, Nucl. Fusion 44 (2004) 699–708.
[4] C. Sozzi, B. Berardi, R. Bozzi, A. Bruschi, G. Ciccone, S. Cirant, et al., High power system for ECRH at 140 Ghz, 2 MW, 0.5 s on FTU tokamak, Am. Inst. Phys. Conf. Proc. 485 (1999) 462–465.
[5] J. Lohr, Y.A. Gorelov, K. Kajiwara, D. Ponce, R.W. Callis, J.L. Doane, et al., The electron cyclotron resonant heating system on the DIII-D tokamak, Fusion Sci. Technol. 48 (2005) 1226–1237.
[6] E. Barbato, ECRH studies: internal transport barriers and MHD stabilization, Plasma Phys. Control. Fusion 43 (2001) A287–A298.
[7] K. Takahashi, K. Kajiwara, A. Kasugai, A. Isayama, Y. Ikeda, S. Ide, et al., High power transmission and polarization measurement in 110 GHz transmission line, Fusion Eng. Des. 53 (2001) 511–516.
[8] J.R. Brandon, S.E. Coe, R.S. Sussmann, K. Sakamoto, R. Sporl, R. Heidinger, et al., Development of CVD diamond r.f. windows for ECRH, Fusion Eng. Des. 53 (2001) 553–559.
[9] L. Rebuffi, J.P. Crenn, Radiation patterns of the HE_{11} mode and Gaussian approximations, Int. J. Infrared Millimeter Waves 10 (1989) 291–311.
[10] M. Lennholm, G. Agarici, G. Berger-By, P. Bosia, F. Bouquey, E. Cellier, et al., The ECRH/ECCD system on Tore Supra, a major step towards continuous operation, Nucl. Fusion 43 (2003) 1458–1476.
[11] J. Zhou, H. Ran, J. Rao, Y. Liu, J. Zhang, S. Song, et al., Design of the ECRH/ECCD launcher system for HL-2A Tokamak, Plasma Sci. Technol. 8 (2006) 344–346.
[12] W. Bin, A. Bruschi, S. Cirant, G. Granucci, S. Mantovani, A. Moro, et al., Design of a new ECRH launcher for FTU Tokamak, Fusion Eng. Des. 84 (2009) 451–456.
[13] H. Kogelnik, T. Li, Laser beams and resonators, Proc. IEEE 54 (1966) 1312–1329.
[14] H.F. Cao, G.L. Mei, Heat Transfer Theory: Theoretical Basis and Engineering Applications, China Communications Press, Beijing, 2006.